

# The nsp3 Macrodomain Promotes Virulence in Mice with Coronavirus-Induced Encephalitis

Anthony R. Fehr,<sup>a</sup> Jeremiah Athmer,<sup>a</sup> Rudragouda Channappanavar,<sup>a</sup> Judith M. Phillips,<sup>c</sup> David K. Meyerholz,<sup>b</sup> Stanley Perlman<sup>a</sup>

Departments of Microbiology<sup>a</sup> and Pathology,<sup>b</sup> University of Iowa, Iowa City, Iowa, USA; Department of Microbiology, Perelman School of Medicine, University of Pennsylvania, Philadelphia, Pennsylvania, USA<sup>c</sup>

## ABSTRACT

All coronaviruses encode a macrodomain containing ADP-ribose-1''-phosphatase (ADRP) activity within the N terminus of non-structural protein 3 (nsp3). Previous work showed that mouse hepatitis virus strain A59 (MHV-A59) with a mutated catalytic site (N1348A) replicated similarly to wild-type virus but was unable to cause acute hepatitis in mice. To determine whether this attenuated phenotype is applicable to multiple disease models, we mutated the catalytic residue in the JHM strain of MHV (JHMV), which causes acute and chronic encephalomyelitis, using a newly developed bacterial artificial chromosome (BAC)-based MHV reverse genetics system. Infection of mice with the macrodomain catalytic point mutant virus (N1347A) resulted in reductions in lethality, weight loss, viral titers, proinflammatory cytokine and chemokine expression, and immune cell infiltration in the brain compared to mice infected with wild-type virus. Specifically, macrophages were most affected, with approximately 2.5-fold fewer macrophages at day 5 postinfection in N1347A-infected brains. Tumor necrosis factor (TNF) and interferon (IFN) signaling were not required for effective host control of mutant virus as all N1347A virus-infected mice survived the infection. However, the adaptive immune system was required for protection since N1347A virus was able to cause lethal encephalitis in RAG1<sup>-/-</sup> (recombination activation gene 1 knockout) mice although disease onset was modestly delayed. Overall, these results indicate that the BAC-based MHV reverse genetics system will be useful for studies of JHMV and expand upon previous studies, showing that the macrodomain is critical for the ability of coronaviruses to evade the immune system and promote viral pathogenesis.

## IMPORTANCE

Coronaviruses are an important cause of human and veterinary diseases worldwide. Viral processes that are conserved across a family are likely to be good targets for the development of antiviral therapeutics and vaccines. The macrodomain is a ubiquitous structural domain and is also conserved among all coronaviruses. The coronavirus macrodomain has ADP-ribose-1''-phosphatase activity; however, its function during infection remains unclear as does the reason that coronaviruses have maintained this enzymatic activity throughout evolution. For MHV, this domain has now been shown to promote multiple types of disease, including hepatitis and encephalitis. These data indicate that this domain is vital for the virus to replicate and cause disease. Understanding the mechanism used by this enzyme to promote viral pathogenesis will open up novel avenues for therapies and may give further insight into the role of macrodomain proteins in the host cell since these proteins are found in all living organisms.

Coronaviruses (CoVs) are a large family of viruses that cause a variety of diseases in mammals and humans, ranging from gastrointestinal and respiratory diseases in veterinary animals (e.g., porcine epidemic diarrhea virus [PEDV] and infectious bronchitis virus [IBV]) to severe respiratory diseases in humans (severe acute respiratory syndrome coronavirus [SARS-CoV] and Middle East respiratory syndrome coronavirus [MERS-CoV]). These viruses often cause severe disease, but no therapeutic drugs and only a few vaccines have been developed to combat coronaviruses. Thus, it is critical to continue to identify potential drug targets and develop novel vaccine platforms and strategies to limit diseases induced by this group of viruses (1, 2).

Coronaviruses are enveloped, positive-stranded RNA viruses that contain the largest known genome size of any class of RNA viruses, ranging from 26 to 32 kb. The viral genome organization is highly conserved, with the nonstructural proteins (nsps) residing in the 5' two-thirds of the genome while the structural and accessory proteins are located in the 3' one-third of the genome. The nonstructural proteins are translated as large polyproteins and contain most of the proteins required for genomic RNA (gRNA) and subgenomic RNA synthesis. In addition, some non-

structural proteins are processing or modulatory proteins that alter the cellular environment to favor efficient replication. Among the nonstructural proteins, coronaviruses code for many proteins with enzymatic activities that rarely occur in other viruses (exoribonuclease [nsp14], endoribonuclease [nsp15], ADP-ribose-1-phosphatase [nsp3], and a deubiquitinase [nsp3]) (1, 2).

In this study, we aimed to further address the role of the macrodomain of nsp3. nsp3 is a large protein consisting of numerous distinct domains separated by disordered linkers. The domains of

Received 9 September 2014 Accepted 15 November 2014

Accepted manuscript posted online 26 November 2014

Citation Fehr AR, Athmer J, Channappanavar R, Phillips JM, Meyerholz DK, Perlman S. 2015. The nsp3 macrodomain promotes virulence in mice with coronavirus-induced encephalitis. *J Virol* 89:1523–1536. doi:10.1128/JVI.02596-14.

Editor: K. Kirkegaard

Address correspondence to Stanley Perlman, stanley-perlman@uiowa.edu.

Copyright © 2015, American Society for Microbiology. All Rights Reserved.

doi:10.1128/JVI.02596-14

nsp3 include, but are not limited to, a ubiquitin-like domain, an acidic domain, a papain-like protease (PL<sup>PRO</sup>) domain, multiple transmembrane domains, and a macrodomain (1, 3). The macrodomain is a globular domain containing central  $\beta$ -sheets flanked by  $\alpha$ -helices that binds to various forms of ADP-ribose (4). This domain is conserved in all living species with 11 macrodomain-containing proteins encoded in the human genome alone (5). A variety of functions have been ascribed to macrodomains, including binding to mono- and poly(ADP-ribose) (MAR-PAR), deacetylating O-acetyl-ADP-ribose, and dephosphorylating ADP-ribose-1''-phosphate (Appr-1''-p) (4). More recently, several groups demonstrated that mammalian, fungal, and archaic macrodomains were capable of removing MAR from ADP-ribosylated proteins (deMARylation) (6–8). While the macrodomain is highly conserved in coronaviruses, it is found in only a few other virus families, most notably the alpha-like supergroup family of viruses, such as Sindbis and Chikungunya viruses (9). The coronavirus macrodomain has highly specific phosphatase activity toward Appr-1''-p *in vitro* and is also known as an ADP-ribose-1''-phosphatase (ADRP) (9). This substrate is produced primarily during cellular tRNA processing during which a 2' phosphate from tRNA is transferred to NAD<sup>+</sup> using a 2' phosphotransferase, resulting in ADP-ribose-1''-2'' cyclic phosphate (10). The cyclic nucleotide is converted to Appr-1''-p by cyclic phosphodiesterase (CPD) and ultimately to ADP-ribose (ADR) by ADRP (11). However, Appr-1''-p has not been detected in coronavirus-infected cells, and, further, there is not a theoretical basis to explain its production during replication. Alternatively, the coronavirus macrodomain may have other enzymatic functions during infection, such as removing MAR from ADP-ribosylated proteins (5–7). In support of this idea, the residues required for deMARylation in human macrodomains are highly conserved in coronaviruses (8). These residues include those required for phosphatase activity, so it is possible that previously identified phenotypes using point mutants could reflect loss of this activity.

Structural studies have described the three-dimensional (3-D) structure of the coronavirus macrodomain and have identified residues involved in substrate binding as well as those essential for ADRP activity (12–15). All of these studies concluded that a completely conserved asparagine residue at the N terminus of this domain (residue 1348 of mouse hepatitis virus strain A59 [MHV-A59]) is the primary catalytic residue in the active site of this enzyme. This has been corroborated by *in vitro* studies of both coronavirus and alphavirus macrodomains showing that a point mutant changing this asparagine to alanine eliminates its phosphatase activity and does not affect its PAR binding ability (9, 12, 15, 16). Virus mutated in the catalytic site replicates similarly to wild-type (WT) virus in tissue culture (9, 17, 18); however, the MHV-A59 mutant virus N1348A is unable to cause hepatitis normally induced by MHV-A59 (18). Additionally, the N1348A mutant was associated with reduced inflammatory cytokine production *in vitro* and *in vivo*. The ADRP domain did not appear to have a role in countering the interferon (IFN) response because the N1348A mutant did not cause hepatitis in IFNAR<sup>-/-</sup> mice and did not have increased sensitivity to interferons compared to wild-type virus (18). Of note, mutation of the catalytic asparagine of the SARS-CoV macrodomain resulted in enhanced sensitivity to IFN, suggesting virus strain or tissue-specific variations in function (17).

Neurotropic strains of MHV, including the JHM strain

(JHMV), cause acute and chronic encephalomyelitis (19). JHMV is highly neurovirulent, with tropism largely confined to the brain. Reverse genetics systems for JHMV have been limited, with targeted recombination the only published approach to introducing mutations into the genome (20). Targeted recombination is useful for manipulation of the 3' end of the viral genome but cannot be used to mutate the nonstructural proteins at the 5' end of the genome. To develop a full-length, infectious cDNA clone useful for introducing mutations into the entire genome, we created a bacterial artificial chromosome (BAC) containing the JHMV genome. BACs offer many advantages for the creation of recombinant coronaviruses (21–23). First, the full-length version of the genome is highly stable in bacteria as BACs are present only in one or two copies per cell. This is especially useful for MHV as this virus is known to contain several sequences that are toxic for bacterial growth when they are present in high copy numbers (24). Second, the cDNA clone can be produced in large quantities, and infection can be launched in a highly efficient manner because transcription originates from a cytomegalovirus (CMV) promoter. This allows viral RNA synthesis to occur in the nucleus following transfection, eliminating the need for the *in vitro* RNA production steps necessary using some other types of coronavirus infectious clones (25). Third, the ability to analyze the BAC clone immediately prior to transfection minimizes the likelihood that undesirable mutations have occurred during production of the clone. Finally, engineering recombinant viruses using BACs is a highly rapid and efficient process in which alterations (i.e., point mutations, deletions, and insertions) can be introduced anywhere in the viral genome. This is achieved by homologous recombination using a two-step procedure that combines linear recombination and counterselection with the endonuclease I-SceI (26).

In this study, we created a novel BAC-based reverse genetics system for JHMV and showed that the BAC was capable of producing infectious virus with replicative and pathogenic properties equivalent to those of other recombinant versions of this virus. We then used homologous recombination to engineer a point mutation of the catalytic asparagine within the macrodomain of nsp3 (N1347A) and characterized the infection caused by this virus in mice.

## MATERIALS AND METHODS

**Cell culture.** 17Cl-1 cells, HeLa cells expressing the MHV receptor carcinoembryonic antigen-related cell adhesion molecule 1 (CEACAM1) (HeLa-MHVR cells), delayed brain tumor (DBT) cells, and baby hamster kidney (BHK) cells were grown as previously described (27).

**Mice.** Pathogen-free C57BL/6 (B6) mice were purchased from the National Cancer Institute (Frederick, MD). IFNAR<sup>-/-</sup>, tumor necrosis factor-negative (TNF<sup>-/-</sup>), and RAG1<sup>-/-</sup> mice were purchased from Jackson Laboratories and bred at the University of Iowa. Mice were maintained in the animal care facility at the University of Iowa. Animal studies were approved by the University of Iowa Animal Care and Use Committee (IACUC).

**Construction of a JHMV BAC.** A synthetic DNA (Genscript) was constructed containing a 5' SmaI site followed by a CMV promoter fused to nucleotides 1 to 1991 and 30314 to 31511 of the JHMV genome and separated by a NotI site (Fig. 1). Fused to the 3' end of the viral sequence was a 25-nucleotide poly(A) stretch, the hepatitis delta virus (HDV) ribozyme and cleavage site, the bovine growth hormone (BGH) termination and polyadenylation sequences, and finally an HindIII site (full sequence available upon request). The pUC57 vector containing this synthetic DNA was digested with SmaI and HindIII while pBeloBAC11 (New Eng-

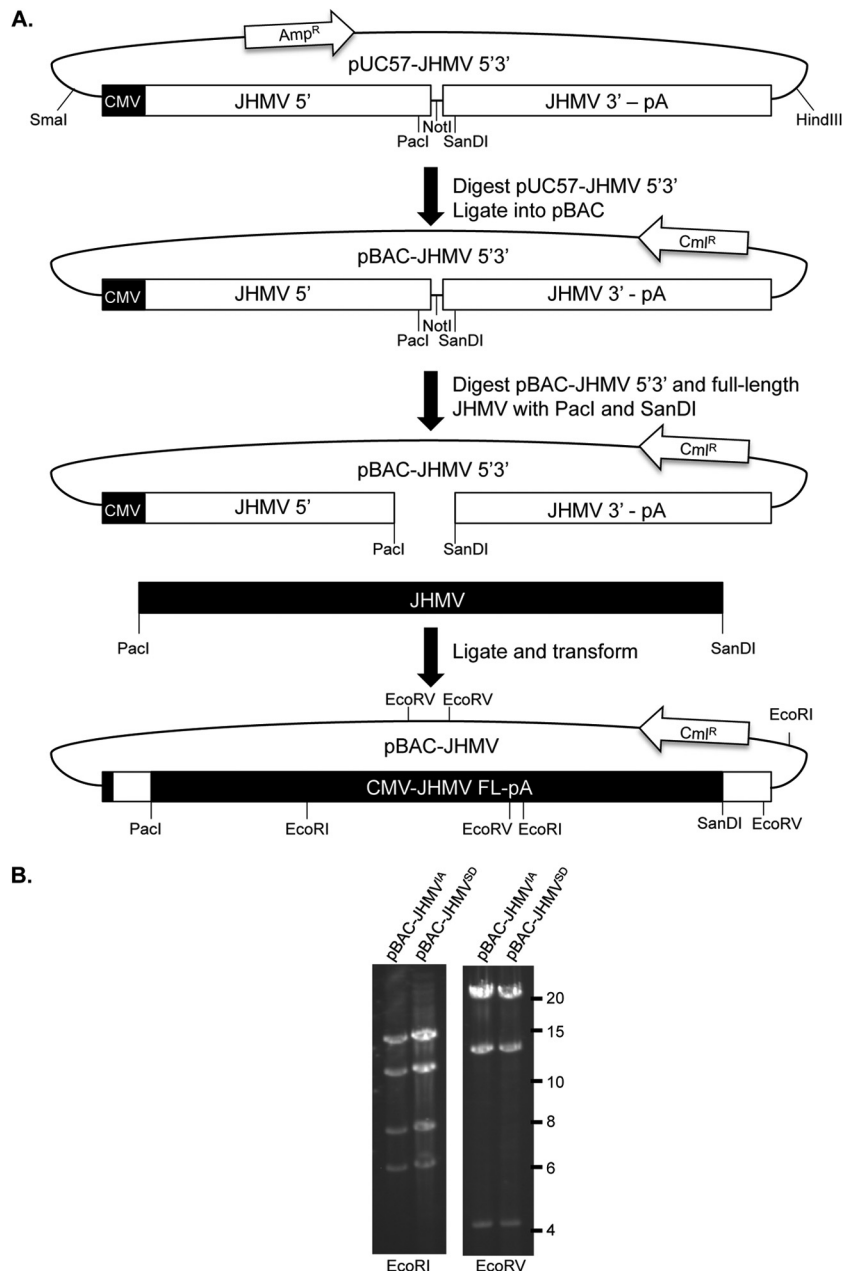


**FIG 1** Engineering a full-length JHMV infectious BAC. (A) Strategy used to construct the JHMV BAC. First, a synthetic DNA was designed containing a CMV promoter, 1,991 bp of 5' JHM sequence, and 1,197 bp of 3' JHM sequence separated by a NotI site, and finally a poly(A) tail (pA), ribozyme cleavage site, HDV ribozyme, and BGH termination signal at the end. This DNA was then digested with SmaI and HindIII and ligated into the parental BAC plasmid, and the resulting clone was termed pBAC-JHMV 5'3'. Subsequently, pBAC-JHMV 5'3' and a full-length JHMV ligated *in vitro* were digested with Pacl and SanDI, ligated, and transformed into competent DH10B *E. coli* cells. The resulting BAC was termed pBAC-JHMV. (B) Confirmation of BAC clones. Representative clones of pBAC-JHMV<sup>IA</sup> and pBAC-JHMV<sup>SD</sup> were digested with EcoRI and EcoRV. The expected banding pattern for EcoRI digestion is 14.5, 11, 7.7, and 6.3 kb, while the expected pattern from EcoRV digestion is 22.3, 12.6, 4.7, and 0.2 kb. The resulting digests matched the expected digestion patterns (0.2-kb fragment is undetectable on the gel).

land BioLabs) was digested with SfoI and HindIII. The SmaI-HindIII fragment was ligated into pBeloBAC11 and transformed into electrocompetent DH10B cells. Transformants were selected on chloramphenicol (Cml)-containing LB plates. The resulting plasmid was named pBAC-JHMV 5'3'. To introduce the remainder of the JHMV genome into pBAC-JHMV 5'3', a full-length DNA fragment of JHMV was created using *in vitro* ligation (unpublished data). Two full-length constructs were created, JHMV Iowa (JHMV<sup>IA</sup>) and a second in which the S protein from

the San Diego (SD) isolate was introduced into the JHMV<sup>IA</sup> background, yielding JHMV<sup>SD</sup>. The ligated full-length genomes and pBAC-JHMV 5'3' construct were then digested with Pacl and SanDI (ThermoScientific), ligated, and transformed back into DH10B cells. Transformants were again selected on LB-chloramphenicol plates, and colonies were screened by PCR and restriction digestion with EcoRI and EcoRV (Fig. 1B). For full-genome sequencing, primers located ~500 bp apart were designed and synthesized (Genscript), and sequences were analyzed using Laser-

TABLE 1 Primers used to create recombinant BAC

Primer description	Sequence <sup>a</sup>	Resulting construct
Forward external primer to amplify GFP-FRT-Kan <sup>r</sup> to replace ORF4 in pBAC-JHMV	5'-TTATAGCATTTTAGTTGCTACTTTGCTCCTCTAGAGGGCAGCAAAGT AGTTATGGGGTCATCCAAGTCAAAAC-3'	pBAC-JHMV-GFP
Reverse external primer to amplify GFP-FRT-Kan <sup>r</sup> to replace ORF4 in pBAC-JHMV	5'-GGACGGCCAGAATTAAGATGAGGTTAGAACTAGTAATATAATCT AGAGTCGTGGAATGCCCTCGAATTC-3'	
Forward internal primer to amplify FRT-Kan <sup>r</sup> with 3' end of GFP sequence	5'-CGACGTGCCTGATTACGCTTGAGAAGTTCCTATTCTCTAGAAAAG-3'	
Reverse internal primer to amplify GFP with FRT site	5'-CTTTCTAGAGAATAGGAAGTCTCAAGCGTAATCAGGCACGTGCG-3'	
Forward primer to amplify N1347A-Kan <sup>r</sup> -I-SceI	5'-TTTGCGCAGAGTTGGTGTGTAAGTCATCGTCAACCCTGCTGCTGG GCGCATGGCTCATGGAGGATGACGACGATAAGTAGGG-3'	pBAC-JHMV <sup>IA</sup> - GFP-N1347A
Reverse primer to amplify N1347A-Kan <sup>r</sup> -I-SceI	5'-TAGCACCTGCAACACCCGCACCATGAGCCATGCGCCCCAGCAGCAG GGTTGACGATGACTTGCCAGTGTACAACCAATTAACC-3'	
Forward primer to amplify revN1347-Kan <sup>r</sup> -I-SceI	5'-TTTGCGCAGAGTTGGTGTGTAAGTCATCGTCAACCCTGCTAATGG GCGCATGGCTCATGGAGGATGACGACGATAAGTAGGG-3'	pBAC-JHMV <sup>IA</sup> - GFPrevN1347
Reverse primer to amplify revN1347-Kan <sup>r</sup> -I-SceI	5'-TAGCACCTGCAACACCCGCACCATGAGCCATGCGCCCCATTAGCAG GGTTGACGATGACTTGCCAGTGTACAACCAATTAACC-3'	

<sup>a</sup> Viral sequences are in italics, marker-specific sequences are in boldface, and specific mutations are underlined.

gene Seqman Pro (primer sequences available upon request). The final BAC constructs were termed pBAC-JHMV<sup>IA</sup> and pBAC-JHMV<sup>SD</sup>.

**Generation of recombinant pBAC-JHMV constructs.** All recombinant pBAC-JHMV constructs were created using Red recombination (primers listed in Table 1). To create a green fluorescent protein (GFP)-expressing BAC, pBAC-JHMV was first transformed into SW105 *Escherichia coli* cells that contain *Flp* recombinase under the control of an arabinose-inducible promoter (a generous gift from Dong Yu, Novartis, Boston, MA) (28). A PCR product containing GFP-FRT-Kan<sup>r</sup>-FRT (where FRT is *Flp* recognition target and Kan<sup>r</sup> indicates the kanamycin resistance gene) and 50 bp of homology to the 5' and 3' regions immediately outside ORF4 of JHMV was created using two-step PCR with external and overlapping internal primers. GFP containing an N-terminal membrane targeting sequence (NTS) was amplified from pUC57-NTS-GFP (Genscript) while FRT-Kan<sup>r</sup>-FRT was amplified from plasmid C006 (a generous gift from Dong Yu). This cassette was then transformed and recombined with pBAC-JHMV replacing ORF4 with GFP-FRT-Kan<sup>r</sup>-FRT. Resulting recombinants were selected on LB-chloramphenicol-kanamycin plates and checked for proper insertion by restriction enzyme digestion and PCR. Correct clones were subsequently amplified and treated with arabinose to induce the *Flp* recombinase and excise the Kan<sup>r</sup> gene, leaving only GFP and an extra 34-bp FRT site at the 3' end of this locus. BAC DNA from Cml<sup>r</sup> Kan<sup>s</sup> colonies was analyzed by restriction enzyme digestion, PCR, and direct sequencing. The resulting BACs were termed pBAC-JHMV<sup>IA</sup>-GFP and pBAC-JHMV<sup>SD</sup>-GFP.

Recombinant BACs with the N1347A point mutation in the nsp3 macrodomain and their wild-type revertants were engineered using the Kan<sup>r</sup>-I-SceI marker cassette for dual positive and negative selection (26). First, pBAC-JHMV<sup>IA</sup>-GFP was transformed into GS1783 *E. coli* cells (a generous gift from Greg Smith, Northwestern University, Chicago, IL), which contain an arabinose-inducible I-SceI restriction enzyme. The I-SceI restriction site is 18 bp long and is not present in the *E. coli* genome. Then, a PCR product was generated containing 40 bp of unique sequence at each end homologous to nsp3 and 20 bp of overlapping sequence containing the desired mutation, AA<sub>4893-4894</sub>GC, using a Kan<sup>r</sup>-I-SceI cassette amplified from the pEP-Kan-I-SceI plasmid (a generous gift from Keith Jarosinski, University of Iowa, Iowa City, IA). The PCR product was transformed into GS1783 cells and recombined with pBAC-JHMV<sup>IA</sup>-GFP. Recombinant BACs were selected on LB-chloramphenicol-kanamycin plates and verified by restriction enzyme digestion and PCR. Correct clones were treated with arabinose during logarithmic growth to induce production of I-SceI, which cleaves the BAC DNA, allowing intramolecular recombination and removal of the Kan<sup>r</sup>-I-SceI marker cassette. BAC DNA from Cml<sup>r</sup> Kan<sup>s</sup> colonies was analyzed by restriction enzyme digest, PCR, and direct sequencing for

isolation of correct clones. Wild-type revertant BACs were engineered by reintroducing the wild-type sequence into the BAC clones containing the N1347A mutation using the same procedure as described above. The resulting BAC clones were termed pBAC-JHMV<sup>IA</sup>-GFP-N1347A and pBAC-JHMV<sup>IA</sup>-GFPrevN1347 (where rev is revertant), respectively.

**Reconstitution of recombinant pBAC-JHMV-derived virus.** Approximately  $2.5 \times 10^6$  DBT cells were transfected with 2  $\mu$ g of pBAC-JHMV DNA and 1  $\mu$ g of pcDNA-MHV-N plasmid using Lipofectamine 2000 (Invitrogen) as a transfection reagent. Viral plaques were evident by 48 to 72 h after transfection. Then recombinant virus underwent two rounds of plaque purification followed by three to four amplification steps to produce sufficient amounts of virus for subsequent experiments. The resulting BAC-derived recombinant JHM (rJ) viruses used in this study were termed rJ<sup>IA</sup>, rJ<sup>SD</sup>, rJ<sup>IA</sup>-GFP, rJ<sup>IA</sup>-GFP-N1347A (N1347A), and rJ<sup>IA</sup>-GFPrevN1347 (revN1347).

**Virus infection.** rJ virus was grown on 17Cl-1 cells, and virus titers were determined on HeLa-MHVR cells as previously described (27). 17Cl-1 cells were infected with rJ at a multiplicity of infection (MOI) of 0.1, unless otherwise stated, and virus from the supernatant and cells was combined prior to determining viral titers. Male mice, 5 to 8 weeks old (unless otherwise indicated), were anesthetized with Avertin and inoculated intranasally with  $3 \times 10^4$  to  $5 \times 10^4$  PFU of rJ<sup>IA</sup> or  $7 \times 10^3$  to  $8 \times 10^3$  PFU of rJ<sup>SD</sup> in a total volume of 12  $\mu$ l. Alternatively, mice were infected intracranially with 750 PFU in a total volume of 30  $\mu$ l. To obtain virus from infected animals, mice were sacrificed and perfused, and brains were collected in phosphate-buffered saline (PBS). Brain tissue was homogenized using a manual homogenizer, cellular debris was removed by centrifugation, and the supernatant titers were determined on HeLa-MHVR cells.

**Isolation of leukocytes from brain tissue.** Leukocytes were isolated from infected brains as previously described (29).

**Flow cytometry.** Brain-derived cells were blocked with 2.4G2 and then incubated with specific monoclonal antibodies (MAbs) or isotype controls. Cells were analyzed using a FACSVers flow cytometer (BD Biosciences, Mountain View, CA). The following monoclonal antibodies were used for these studies: CD45-phycoerythrin (PE)-Cy7 (30-F11; BD Biosciences), CD11b-peridinin chlorophyll protein (Percp)-Cy5.5 (M1/70; BD Biosciences), Ly6C-allophycocyanin (APC) (AL-21; BD Biosciences), Ly6G-PE (1A8; BD Biosciences), F4/80-PE (BM8; eBioscience), and CD11c-eFluor 450 (N418; eBioscience). All flow cytometry data were analyzed using FlowJo software (Tree Star, Inc., Ashland, OR).

**Real-time qPCR analysis.** RNA was isolated from 17Cl-1 cells or from brain homogenates using TRIzol (Invitrogen) and cDNA prepared as previously described (30). Reverse transcription-quantitative PCR (RT-

TABLE 2 Quantitative real-time PCR primers

Gene	Primer
MHV nsp12	5'-AGGGAGTTTGACCTTGTCAG-3' 5'-ATAATGCACCTGTATCCTCG-3'
HPRT	5'-GCGTCGTGATTAGCGATGATG-3' 5'-CTCGAGCAAGTCTTTCAGTCC-3'
IFN- $\beta$	5'-CCCTATGGAGATGACGGAGA-3' 5'-ACCCAGTGCTGGAGAAATTG-3'
CCL2	5'-CTTCTGGCCTGCTGTTACAGTTGC-3' 5'-GGATGCATTAGCTTCAGATTTACGG-3'
IL-6	5'-GCTACCAAAGTGGATATAATCAGGA-3' 5'-CCAGGTAGCTATGGTACTCCAGAA-3'
TNF- $\alpha$	5'-TCAGCCGATTGCTATCTCA-3' 5'-CGGACTCCGCAAAGTCTAAG-3'

qPCR) was performed using an Applied Biosystems 7300 real-time PCR system (Applied Biosystems, Foster City, CA) using RT<sup>2</sup> 2 $\times$  SYBR green qPCR master mix (Qiagen). Primers used for qPCR are listed in Table 2. Cycle threshold ( $C_T$ ) values were normalized to those of the housekeeping gene hypoxanthine phosphoribosyltransferase (HPRT) by the following equation:  $C_T = C_{T(\text{gene of interest})} - C_{T(\text{HPRT})}$ . All results are shown as a ratio to HPRT calculated as  $-2^{-C_T}$ .

**Histology.** Zinc formalin-fixed brain tissue was embedded in paraffin and sectioned sagittally at a thickness of 8  $\mu$ m. Tissue sections were stained with hematoxylin and eosin (H&E) and assessed by light microscopy.

**Statistics.** Student's *t* test was used to analyze differences in mean values between groups. All results are expressed as means  $\pm$  standard errors of the means (SEM). *P* values of  $\leq 0.05$  were considered statistically significant.

## RESULTS

**Constructing an infectious JHMV BAC.** Reverse genetics systems capable of altering the 5' end of JHMV are limited, so we developed an infectious cDNA clone under the control of the CMV promoter as a BAC (Fig. 1). This system allows the intracellular production of viral RNA without *in vitro* ligation or transcription steps. The JHMV BAC clone was created in several steps, as depicted in Fig. 1A. First, an intermediate BAC was created containing the first 1,991 nucleotides of the JHM virus genome fused to a CMV promoter, a NotI site, and the last 1,197 nucleotides of the genome. In addition, the BAC clone contains a 25-nucleotide poly(A) stretch, the hepatitis delta virus (HDV) ribozyme, and bovine growth hormone (BGH) termination and polyadenylation sequences to maintain a wild-type-like 3' end of the genome (21–23). Further, the intermediate BAC contains unique PacI and SanDI restriction enzyme recognition sites. Full-length JHMV cDNA was then created by ligating seven separate fragments of viral DNA digested with type II restriction endonucleases (unpublished data). The intermediate BAC and full-length JHMV cDNA were digested with PacI and SanDI restriction enzymes, ligated, and then transformed into DH10B *E. coli* cells. Individual clones were screened by restriction endonuclease analysis with EcoRI and EcoRV (Fig. 1B). Two different isolates of JHMV were created as BACs, pBAC-JHMV<sup>IA</sup> and pBAC-JHMV<sup>SD</sup>. pBAC-JHMV<sup>SD</sup> created on the JHMV<sup>IA</sup> background contains the S protein from the natural JHMV<sup>SD</sup> isolate. These isolates differ by 4 amino acids in the S protein but have slightly different phenotypes *in vitro* and *in vivo*. Specifically, JHMV<sup>IA</sup> replicates better in tissue culture but has slightly reduced virulence compared to JHMV<sup>SD</sup> *in vivo* (31).

During screening, it was noted that only the smaller colonies contained the entire JHMV genome, consistent with the notion that certain JHMV sequences diminished the growth of the *E. coli* and that their deletion enhanced growth. To prevent the loss of the full-length BACs, *E. coli* bacteria were grown only at room temperature. All of the BACs were stable at room temperature as we observed no alterations in the BACs after several passages in *E. coli*. Finally, three BAC clones that produced virus, i.e., one JHMV<sup>IA</sup> and two JHMV<sup>SD</sup> clones, were fully sequenced by Sanger sequencing using primers spaced approximately 500 nucleotides apart across the viral genome. All three clones perfectly matched the reference sequences (GenBank accession number AC\_000192.1), indicating that no mutations arose during the construction and passage of the BACs.

**Rescue of infectious rJ from BAC clones.** To produce recombinant JHM (rJ) virus from the BAC clones, we transfected BAC DNA along with the MHV N protein-expressing plasmid into DBT cells (Fig. 2A). Plaques were observed 48 to 72 h after transfection and were identical in morphology and size to those of the control rJ virus. Importantly, plaques were rarely observed in the absence of N protein-expressing plasmid, as previously shown in other coronavirus reverse genetics systems using *in vitro* ligation and transcription to launch virus replication (24, 32, 33). Notably, this is the first CoV BAC that requires N for efficient virus launch. However, whether this is virus specific or dependent on the type of genetic system being used remains unclear. At 72 h, cells and supernatants were collected and used to reinfect 17Cl-1 cells. The virus then underwent two rounds of plaque purification, followed by two to three passages on 17Cl-1 cells. At least two different plaque isolates were obtained for each clone. Virus recovered after five to six passages typically had titers of approximately  $5 \times 10^6$  PFU/ml for the rJ<sup>IA</sup> isolate and  $5 \times 10^5$  PFU/ml for the rJ<sup>SD</sup> isolate.

The recovered viruses were then analyzed for their ability to replicate in tissue culture cells and their ability to cause lethal encephalitis in mice. The BAC-derived virus was compared to other recombinant versions of rJ<sup>IA</sup> and rJ<sup>SD</sup> viruses constructed using targeted recombination or *in vitro* ligation, respectively (20) (unpublished data). For the *in vitro* growth analysis, 17Cl-1 cells were infected at an MOI of 0.1 PFU/cell, and both the cells and supernatants were collected. Both BAC-derived rJ isolates replicated with similar kinetics and reached similar peak titers as their controls although a slight delay was noted with the BAC-derived rJ<sup>IA</sup> viruses (Fig. 2B and C). To analyze viral pathogenesis, 5- to 6-week-old male B6 mice were infected by intranasal inoculation with approximately  $3 \times 10^4$  or  $8 \times 10^3$  PFU of rJ<sup>IA</sup> or rJ<sup>SD</sup>, respectively. Mice were monitored daily for survival (Fig. 3A and B) and weight loss (Fig. 3C and D). Again, as expected, the BAC-derived viruses were able to cause disease as efficiently as the controls, causing lethal encephalitis in all mice at 6 to 10 days postinfection (p.i.) (34).

**Generation of rJ<sup>IA</sup> virus encoding a macrodomain catalytic mutant using linear recombination.** To introduce insertions, deletions, or point mutations into pBAC-JHMV, we used Red recombination in concert with either an arabinose-inducible *flp* recombinase or the homing endonuclease I-SceI (26, 28). Only pBAC-JHMV<sup>IA</sup> was used in subsequent studies. First, GFP was inserted in place of ORF4, a gene that is not required for viral replication in tissue culture or in mice (35), using the arabinose-inducible *flp* recombinase (pBAC-JHMV<sup>IA</sup>-GFP). The GFP insertion along with a 34-bp FRT site left following recombination had

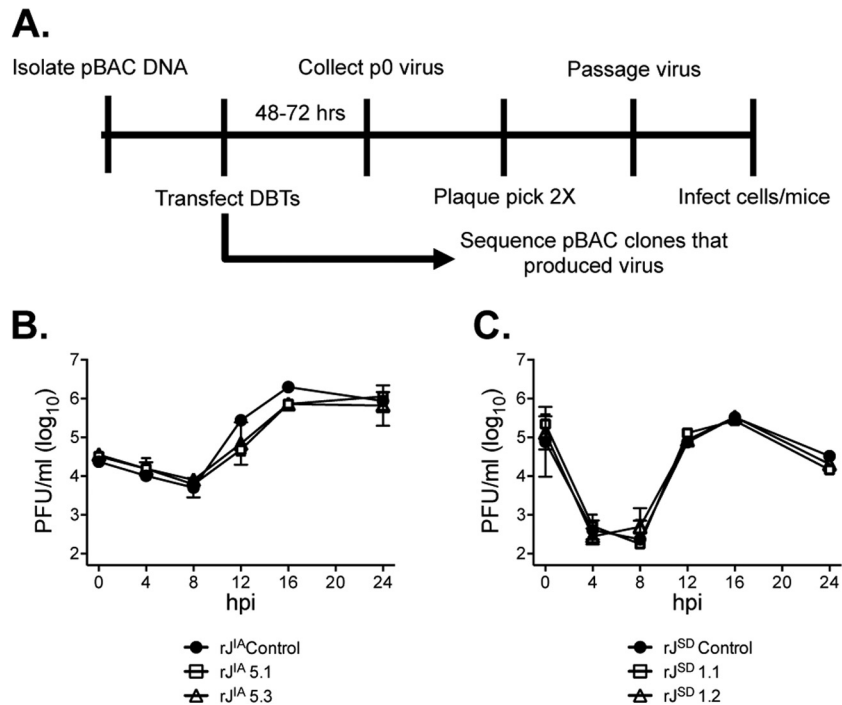


**FIG 2** rJ virus engineered using pBAC-JHMV is infectious and replicates in a similar manner to other recombinant JHMVs. (A) Strategy for creating and recovering rJ virus from BAC clones. pBAC-JHMV DNA was transfected into DBT cells along with a plasmid expressing N protein. After plaques were visible (48 to 72 hpi), the virus was plaque purified two times and passed two to three times on 17Cl-1 cells as described in Materials and Methods. (B and C) Recovered rJ<sup>IA</sup> (B) and rJ<sup>SD</sup> (C) viruses were analyzed for *in vitro* replication on 17Cl-1 cells. Progeny virus was collected at the indicated times postinfection, and yields were determined by plaque assay. p0, passage zero. Numbers in the legends indicate two distinct virus plaque isolates.

little to no effect on viral replication on 17Cl-1 cells compared to the WT recombinant control not expressing GFP (GFP<sup>-</sup>) (Fig. 4A). All other recombinant BACs created in this study used pBAC-JHMV<sup>IA</sup>-GFP as the parental clone.

To generate a point mutant in the catalytic residue of the JHMV macrodomain (N1347A), two-step Red recombination with the endonuclease I-SceI was utilized. This system was initially developed by Tischer et al., and the general strategy is depicted in Fig. 4B (26). Briefly, a PCR product containing a Kan<sup>r</sup>-I-SceI marker cassette flanked with overlapping sequence containing the desired mutation was inserted into the genome by intermolecular recombination. Then the I-SceI restriction enzyme was induced by arabinose, cleaving the I-SceI site in the marker cassette. This allowed for intramolecular recombination, removing the marker cassette and resulting in a BAC that now contained the desired mutation (pBAC-JHMV<sup>IA</sup>-GFP-N1347A). To control for any second-site mutations that might have occurred during recombination and outgrowth of the bacteria, the wild-type sequence was reintroduced back into the mutant BAC clone using the same procedure, recreating a wild-type revertant BAC (pBAC-JHMV<sup>IA</sup>-GFP<sup>rev</sup>N1347). For simplicity, the viruses derived from the recombinant BACs will be termed WT (GFP<sup>-</sup>), WT (GFP<sup>+</sup>) for the WT virus expressing GFP, N1347A, and revN1347 throughout the rest of the manuscript. Also, N1347A and revN1347 viruses express GFP even though this is not included in the shortened notation.

**N1347A is minimally attenuated in tissue culture.** *In vitro* growth kinetics was determined on 17Cl-1 cells, infecting cells with the recombinant viruses at an MOI of 0.1 PFU/cell. First, we

compared WT (GFP<sup>+</sup>) virus to revN1347 (which also expresses GFP) and found that these viruses replicated equivalently (Fig. 4C, left panel). This suggests that no second-site mutation that affected *in vitro* viral growth occurred during production of the BACs. To compare revN1347 and N1347A, two separate clones of each virus were grown out and used in these assays. While all four viruses reached similar peak titers, N1347A had a small but highly reproducible and statistically significant delay in virus production at 12 to 16 h postinfection (hpi) (Fig. 4C, right panel). The difference in viral titers at 12 hpi reached 2- to 4-fold. To determine if differences in viral genomic RNA (gRNA) accumulation could also be detected, we measured viral gRNA levels by reverse transcription-quantitative PCR (RT-qPCR) using specific primers (Table 2). Again, there was approximately 2-fold more viral gRNA in revN1347-infected cells than in N1347A-infected cells (Fig. 4D). No significant difference in viral gRNA levels at 0 hpi was observed, and thus the gRNA (at 0 hpi)-to-PFU ratios of the two viruses were nearly identical (Fig. 4E). To further compare the two viruses, a competition assay was performed in which 17Cl-1 cells were coinfecting with N1347A (GFP<sup>+</sup>) and WT (GFP<sup>-</sup>) virus at an initial infection ratio of ~4:1. We infected cells at a total MOI of 0.1 PFU/cell to largely prevent dual infection of cells. Furthermore, virus titers were determined after each passage to ensure that cells were infected at the same MOI for each passage. To differentiate the two viruses over several passages, the percentage of GFP plaques was determined as only the N1347A virus codes for GFP. As a control, cells were coinfecting with WT (GFP<sup>+</sup>) and WT (GFP<sup>-</sup>) virus at the same initial ratio of ~4:1. N1347A was rapidly outcompeted by WT (GFP<sup>-</sup>) virus so that by passage 3

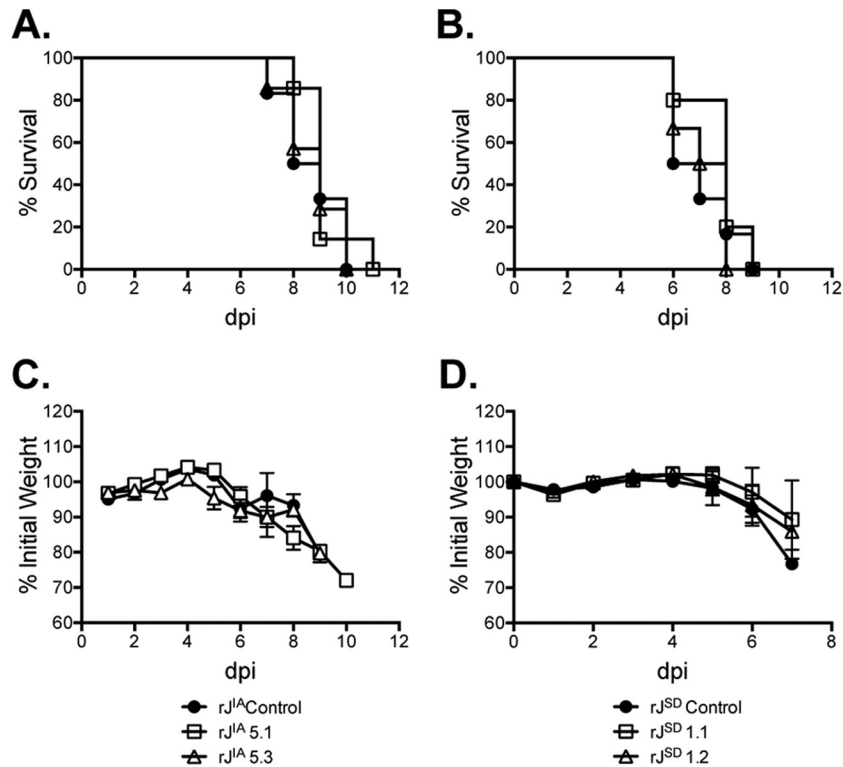


**FIG 3** BAC-derived rJ retains the *in vivo* neurovirulence of other recombinant JHMV. Wild-type B6 mice were infected with 4E4 PFU rJ<sup>IA</sup> (A and C) and 8E3 PFU rJ<sup>SD</sup> (B and D) intranasally and monitored for survival and weight loss daily for 12 days. rJ<sup>IA</sup> and rJ<sup>SD</sup> controls refer to viruses constructed using targeted recombination and *in vitro* ligation, respectively. Data were combined from two independent experiments. rJ<sup>SD</sup> 1.1,  $n = 5$ ; rJ<sup>IA</sup> control, rJ<sup>SD</sup> control, and rJ<sup>SD</sup> 1.2,  $n = 6$ ; rJ<sup>IA</sup> 5.1 and rJ<sup>IA</sup> 5.3,  $n = 7$ . dpi, days postinfection.

only 10% of plaques were GFP positive. In contrast, the WT (GFP<sup>+</sup>) virus was nearly as fit as WT (GFP<sup>-</sup>) virus, with 67% of plaques remaining GFP<sup>+</sup> after 3 passages in the dual infection (Fig. 4D). To confirm continued GFP expression during propagation, we passaged both WT (GFP<sup>+</sup>) and N1347A (GFP<sup>+</sup>) over three passages in the absence of competitor virus and did not observe any loss of GFP expression (data not shown). These data suggest that the N1347A mutant virus is minimally attenuated in tissue culture, with a slight defect in viral gRNA accumulation.

**rJ macrodomain is essential for virus-induced encephalitis in wild-type B6 mice.** Next, we determined whether the N1347A mutant virus was attenuated *in vivo* since it was only minimally attenuated *in vitro*. We infected mice intranasally with approximately  $4 \times 10^4$  PFU of revN1347 or N1347A virus. Consistent with results using macrodomain-mutated MHV-A59 (18), the JHMV N1347A mutant caused no weight loss or lethality, in stark contrast to revN1347 virus (Fig. 5A and B). Brain homogenates were then prepared at days 5 and 7 postinfection, and viral titers in the brain were measured. Indeed, there was about 10-fold less virus in N1347A- than in revN1347-infected brains (Fig. 5C).

When virus is administered intranasally, the virus must spread from the olfactory nerve transneuronally to infect secondary, tertiary, and distal sites in the brain (36). To determine whether the mutant virus was simply attenuated in its ability to invade the brain, virus was also delivered via direct intracranial inoculation. Mice were monitored for survival, weight loss, and viral titers (Fig. 5D to F). N1347A virus was not completely attenuated using this

route of infection since mice exhibited modest weight loss and showed signs of disease, such as mild hunching and ruffled fur. However, all of these mice ultimately survived the infection. In contrast, revN1347-infected mice were moribund by 6 days p.i., losing 25% of their body weight; virus titers in the brain were 4-fold higher than observed in N1347A-infected animals at day 5 p.i. Overall, these data demonstrate that the N1347A virus is attenuated regardless of the route of infection.

**N1347A virus induces lower cytokine and chemokine expression levels and reduced infiltration of innate immune cells and causes only limited pathology in the brains of infected mice.** Next, to determine whether diminished virus replication correlated with an altered innate immune response, we measured the levels of several proinflammatory cytokine and chemokine mRNAs in the brain by RT-qPCR following infection with revN1347 and N1347A viruses. The RNA expression of CCL2, beta interferon (IFN- $\beta$ ), interleukin-6 (IL-6), and TNF- $\alpha$  were all reduced 2- to 4-fold at 5 days p.i. following infection with N1347A virus (Fig. 6A), and all but TNF- $\alpha$  were induced by both viruses compared to naive mice (Fig. 6A). In subsequent analyses, we observed reduced numbers of infiltrating CD45<sup>+</sup> cells in the brains of N1347A-infected mice compared to revN1347-infected mice (Fig. 6C; gating shown in B). While the percentages of each cell type did not vary substantially (only macrophages were significantly different), the numbers of macrophages were 2- to 3-fold higher during revN1347 infection than N1347A infection (Fig. 6C). In contrast, microglia and neutrophil numbers were only slightly reduced in N1347A-infected mice (Fig. 6C). As expected,

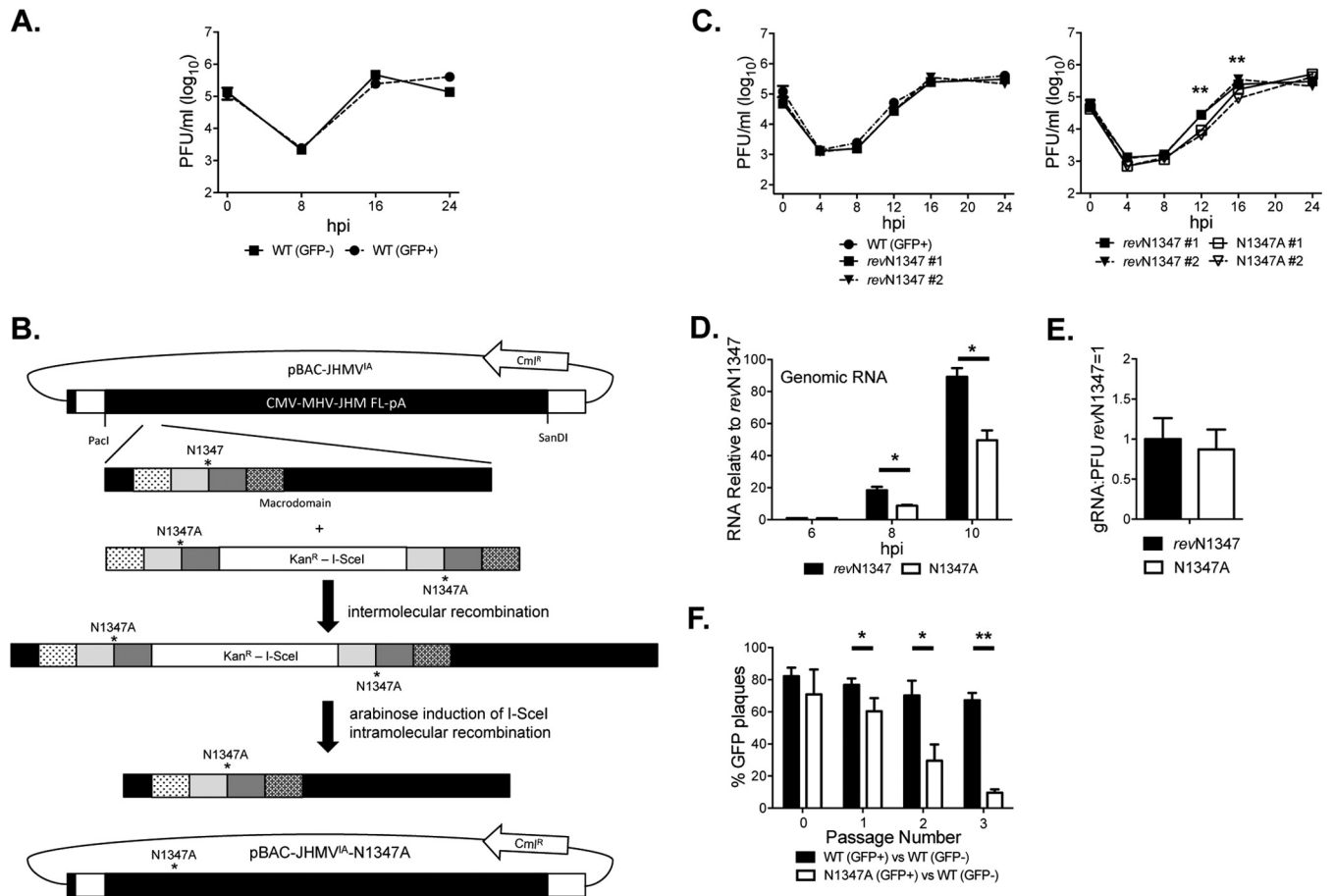


**FIG 4** rJ virus mutant at residue 1347 (N1347A) is minimally attenuated *in vitro*. (A) To compare replication kinetics of WT (GFP<sup>-</sup>) and WT (GFP<sup>+</sup>) viruses, 17Cl-1 cells were infected at an MOI of 0.1 PFU/cell. Progeny virus was collected at the indicated times postinfection, and titers were determined by plaque assay. (B) pBAC-JHMV encoding the N1347A mutant was created using a two-step linear recombination with a Kan<sup>R</sup>-I-SceI dual marker cassette as described in Materials and Methods. Individually shaded boxes indicate regions of homology to viral sequence; the asterisk identifies the location of the active-site asparagine. Revertant rJ was also engineered (revN1347) using the same procedure. (C) Growth kinetics of rJ<sup>ΔA</sup>. 17Cl-1 cells were infected with the indicated viruses. Progeny virus was collected at the indicated times postinfection, and yields were determined by plaque assay. (D) To assess RNA accumulation, 17Cl-1 cells were infected with the indicated viruses, and total RNA was collected at the indicated times postinfection. RNA was quantified by RT-qPCR with primers specific for genomic RNA and normalized to HPRT (Table 2 lists qPCR primers). The normalized amount of viral transcript at 6 hpi during revN1347 infection was set to 1. (E) Viral genome RNA/PFU ratio was determined by dividing the relative gRNA of revN1347 and N1347A virus from cells at 0 hpi by the PFU count of the viral stocks. The normalized ratio of revN1347 virus was set to 1. Data shown are mean values and standard errors of the means from two independent experiments with two different virus stocks performed in duplicate. (F) To examine viral fitness *in vitro*, 17Cl-1 cells were coinfecting with N1347A (GFP<sup>+</sup>) and wild-type (GFP<sup>-</sup>) virus or wild-type (GFP<sup>+</sup>) and wild-type (GFP<sup>-</sup>) virus at a ratio of ~4:1 and at a combined MOI of 0.1 PFU/ml. Virus was passed three times in 17Cl-1 cells, with titers determined after each passage so that at each subsequent passage cells were infected at an MOI of 0.1 PFU/cell. The percentage of GFP-expressing virus was determined by dividing the number of GFP<sup>+</sup> plaques by the number of total plaques. Passage 0 represents input virus. Data shown are mean values ± standard errors of the means (SEM) from a representative experiment performed in duplicate. \*,  $P \leq 0.05$ ; \*\*,  $P \leq 0.005$ .

macrophages were largely positive for Ly6C (data not shown), consistent with their hematogenous origin (37). Lower proinflammatory cytokine and chemokine expression and reduced recruitment of bone marrow macrophages into the brains of N1347A-infected mice likely played a role in the reduced severity of encephalitis observed in these animals (38). Furthermore, to demonstrate brain pathology, we analyzed brains from intranasally infected mice at 7 days p.i. by H&E staining. Mice infected with N1347A virus displayed occasional perivascular infiltrates but otherwise were devoid of any significant signs of pathology (Fig. 6D and E). However, revN1347-infected mice displayed increased perivascular infiltrates, cellular debris, and apoptotic cells, consistent with brain disease typically induced by JHMV (Fig. 6F to G).

### The role of innate immune signaling in JHMV infection.

Type 1 IFN is critical for protection against all strains of MHV (39, 40). To determine whether IFN signaling was required for protection against N1347A, we infected IFN- $\alpha/\beta$  receptor-negative (IFNAR<sup>-/-</sup>) mice with revN1347 or N1347A intranasally and analyzed them for survival and weight loss (Fig. 7A and C). In IFNAR<sup>-/-</sup> mice, N1347A virus was unable to cause lethal encephalitis (Fig. 7A) but did induce significant weight loss compared to wild-type mice (Fig. 7C; compare to 5B). To determine if these differences reflect differences in IFN sensitivity, 17Cl-1 cells were treated with IFN- $\beta$  and infected with revN1347 or N1347A. N1347A retained the same sensitivity to IFN as revN1347, with 100 U of IFN- $\beta$  reducing titers of both viruses approximately 2 logs (Fig. 7E). We also infected TNF<sup>-/-</sup> mice with the two viruses.

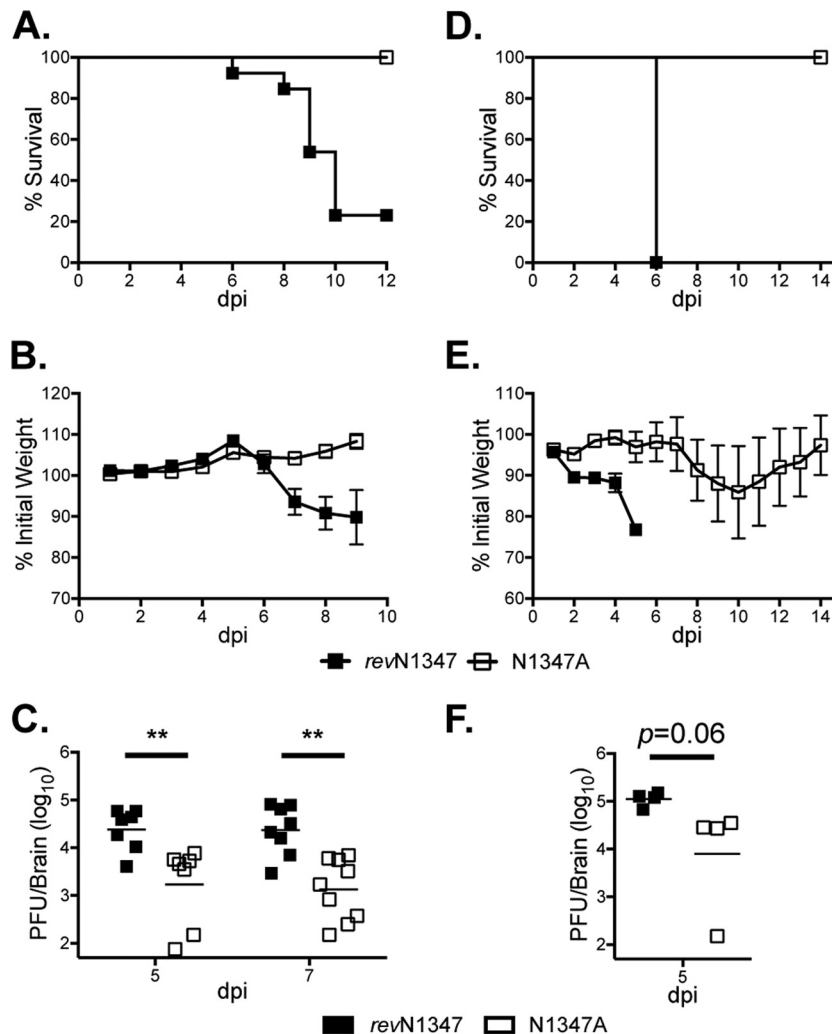


**FIG 5** N1347A is attenuated in wild-type mice. (A and B) Wild-type B6 mice were infected intranasally with the indicated viruses and monitored daily for survival and weight loss. Weight curves were terminated at day 9 as most revN1347-infected mice had succumbed to infection by this point. Data are combined from two independent experiments ( $n = 13$  in the revN1347 group and  $n = 14$  in the N1347A group). (C) To determine virus load in the brains of infected mice, B6 mice were infected intranasally, and brains were homogenized at 5 and 7 days p.i. Homogenates were clarified by centrifugation, and titers were determined by plaque assay. Viral titers are expressed as the number of PFU/brain. Data were combined from two independent experiments ( $n = 7$  per group at 5 days p.i. and  $n = 9$  or 8 in the revN1347 or N1347A group, respectively, at 7 days p.i.). Lines represent mean values. (D and E) B6 mice were infected intracranially and monitored for survival and weight loss for 14 days ( $n = 3$  mice per group). (F) Analysis of virus loads in the brains of intracranially infected mice. Brains were harvested at the indicated times and analyzed for viral loads as described for panel C. In panels C and F, the x axis indicates the limit of detection. Data were combined from two independent experiments ( $n = 4$  per group). \*,  $P \leq 0.05$ ; \*\*,  $P \leq 0.005$ .

revN1347 virus caused similarly lethal infections in  $TNF^{-/-}$  and B6 mice (Fig. 7B), but, remarkably,  $TNF^{-/-}$  mice succumbed to infection without losing weight (Fig. 7D), indicating that TNF was involved in mediating the weight loss observed in these mice. Importantly, N1347A was still unable to cause disease in  $TNF^{-/-}$  mice (Fig. 7B and D), showing that TNF signaling does not contribute to its attenuation.

**Increased mortality in mice lacking T and B cells.** In general, a potent antiviral T cell response is required for coronavirus clearance (41, 42). Accordingly, even attenuated strains of JHMV are able to persist for several weeks in  $RAG1^{-/-}$  mice, which lack T and B cells (43). As expected,  $RAG1^{-/-}$  mice infected with revN1347 developed a lethal infection. Surprisingly, mice infected with N1347A also lost a significant amount of weight, and greater than 50% ultimately succumbed to infection, albeit in a delayed

manner (Fig. 8A and B). Interestingly, N1347A-infected mice that were moribund displayed high virus loads at 12 days p.i. ( $>10^5$  PFU/brain), while those that survived the infection had cleared the virus at 14 days p.i. (Fig. 8C).

Collectively, these results show that N1347A is sufficiently attenuated so that virus is cleared, and the mice develop only mild disease in the absence of IFN signaling; however, if the virus is able to persist, as in  $RAG1^{-/-}$  mice, it is able to cause a lethal disease.

## DISCUSSION

It is well established that coronaviruses and viruses in the alpha-like supergroup of positive-strand RNA viruses contain a highly conserved macrodomain. However, the role, function, and purpose of this domain in the context of viral replication and pathogenesis have remained enigmatic. Previous studies have largely

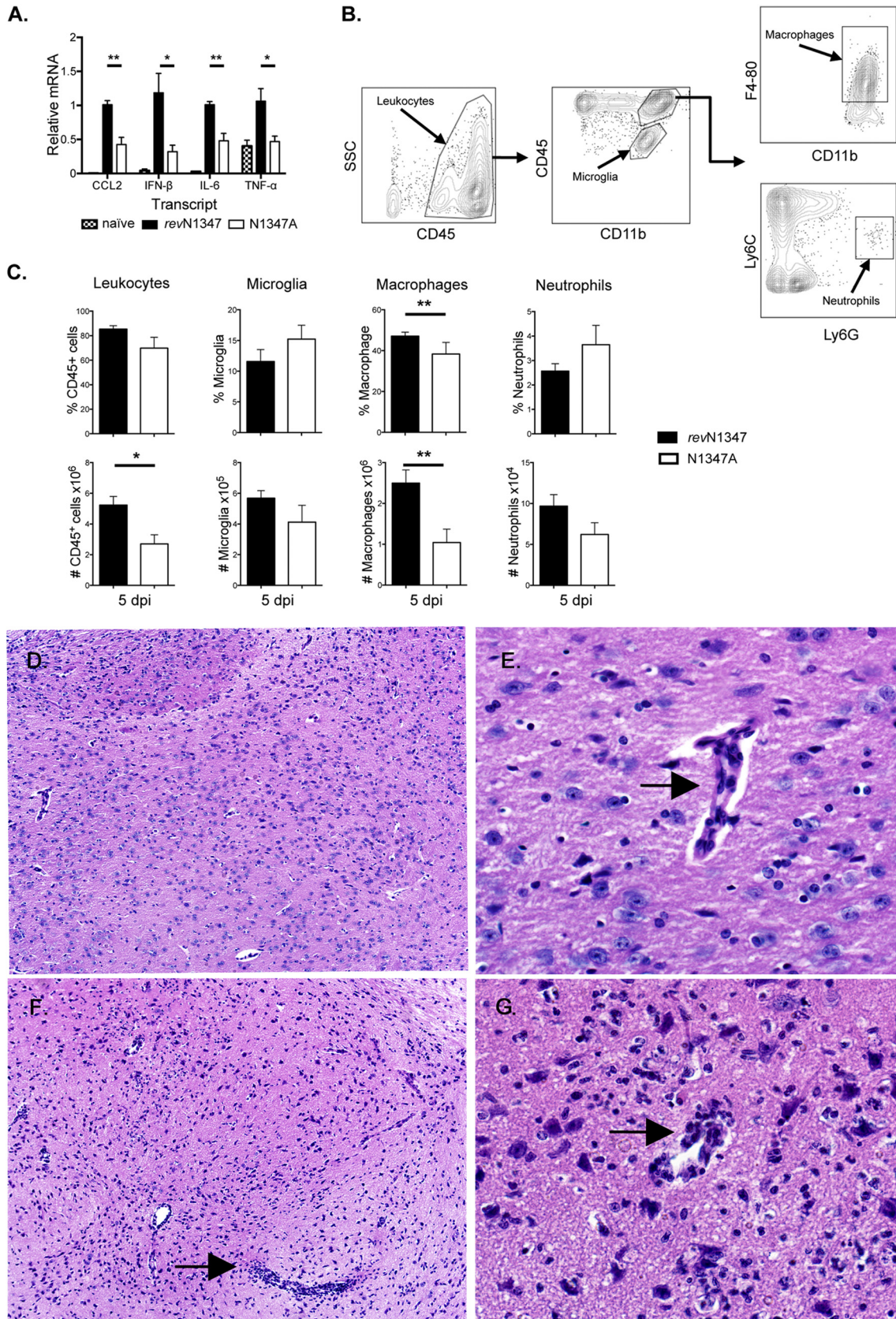
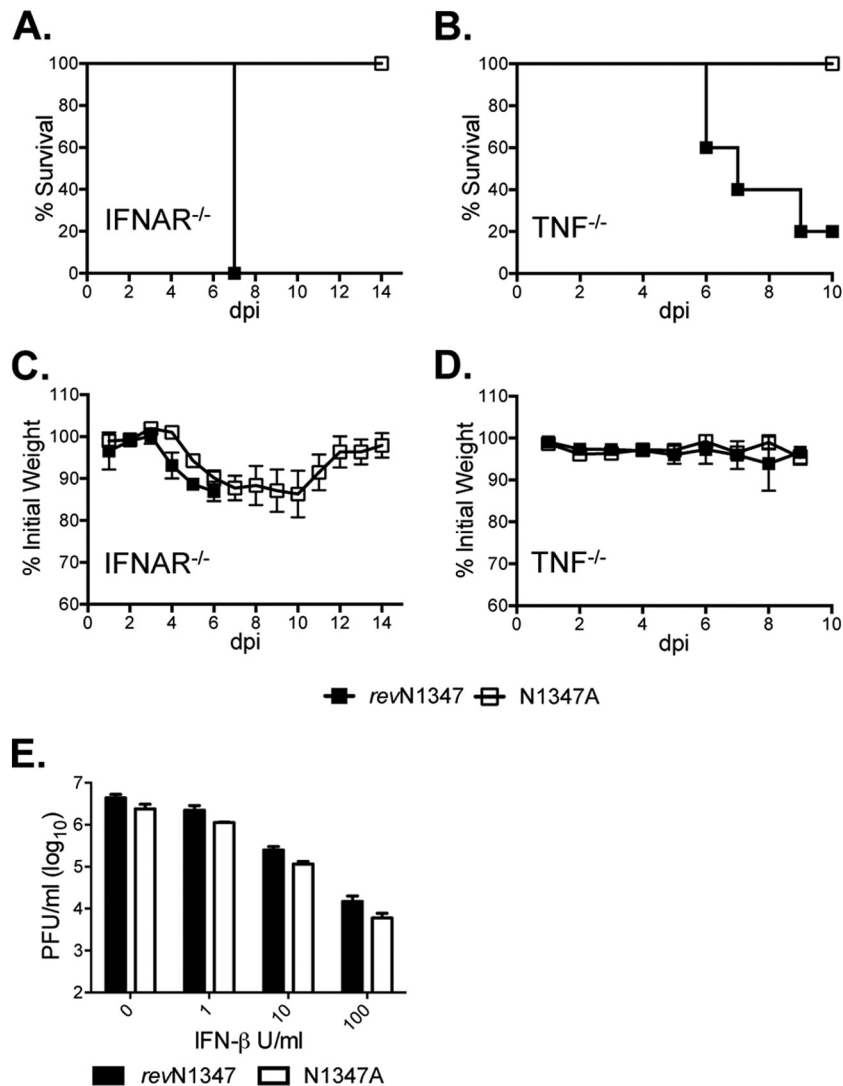


FIG 6 N1347A induces lower levels of proinflammatory cytokine and chemokine gene expression than revN1347 and reduced recruitment of immune cells into the brain and causes limited pathology in brains of infected mice. (A) To analyze proinflammatory cytokine and chemokine expression following infection,



**FIG 7** N1347A is attenuated in *IFNAR*<sup>-/-</sup> and *TNF*<sup>-/-</sup> mice. Eight-week-old *IFNAR*<sup>-/-</sup> (A and C) or 4- to 5-month-old *TNF*<sup>-/-</sup> (B and D) male mice were infected intranasally with revN1347 and N1347A viruses and monitored daily for survival and weight loss for 10 or 14 days, respectively, as indicated. For the experiments shown in panels A and C,  $n = 3$  for the revN1347 infection group, and  $n = 5$  for the N1347A infection group; for the experiments shown in panels B and D,  $n = 5$  for the revN1347 infection group, and  $n = 4$  for the N1347A infection group. Combined results from two independent experiments are shown. (E) N1347A does not have increased sensitivity to IFN compared to revN1347 virus. I7C1-1 cells were pretreated with the indicated amounts of IFN- $\beta$  (PBL, Piscataway, NJ) for 18 h, infected with revN1347 virus and N1347A virus at an MOI of 0.1 PFU/cell, and posttreated with IFN. Cells were analyzed for infectious virus at 20 hpi by plaque assay. Data are representative of two independent experiments.

found that this domain is nonessential for replication *in vitro* but may be important for *in vivo* pathogenesis (9, 17, 18). Specifically, viruses with mutations in the catalytic site in the macrodomain of MHV-A59 or Sindbis virus were unable to cause hepatitis or had

reduced neurovirulence, respectively (16, 18). In accordance with these results, we found that rJ virus mutated in the catalytic site (N1347A) was also severely attenuated *in vivo* and unable to cause lethal encephalitis in B6 mice.

B6 mice were infected intranasally with revN1347 and N1347A viruses, and total brain RNA was collected at 5 days p.i. RNA was quantified by RT-qPCR with primers specific for CCL2, IFN- $\beta$ , IL-6, TNF, and HPRT (Table 2 lists qPCR primers). The normalized amount of viral transcript in revN1347-infected mice was set to 1 ( $n = 6$  for revN1347- and N1347A-infected mice;  $n = 3$  for naive mice). Combined results from two independent experiments are shown. (B) Gating strategy for identifying leukocytes (CD45<sup>+</sup>), microglia (expressing intermediate levels of CD45 [CD45<sup>int</sup>] and CD11b<sup>+</sup>), macrophages (expressing high levels of CD45 [CD45<sup>high</sup>], CD11b<sup>+</sup>, and F4-80<sup>+</sup>), and neutrophils (CD45<sup>high</sup> CD11b<sup>+</sup> Ly6C<sup>+</sup> Ly6G<sup>+</sup>) from intranasally infected mice is shown. (C) Frequencies (upper panel) and cell numbers (lower panel) of total leukocytes, macrophages, microglia, and neutrophils are shown. Percentages of CD45<sup>+</sup> cells are determined from the total cell population, while percentages for the individual cell populations refer to the CD45<sup>+</sup> population ( $n = 5$  for each group). Results are representative of two independent experiments. \*,  $P \leq 0.05$ ; \*\*,  $P \leq 0.005$ . (D to G) Histological analysis of brains from mice infected intranasally with N1347A (D and E) or revN1347 (F and G) at 7 days p.i. Sections were prepared from the brainstems of infected mice and stained with hematoxylin and eosin. Foci of increased cellularity with apoptotic cells and cellular debris were detected primarily in revN1347-infected mice although perivascular infiltrates were found in mice infected with either virus. A region of the midbrain is shown in the figure. Black arrows indicate perivascular infiltrates. Original magnifications,  $\times 100$  (D and F) and  $\times 400$  (E and G).  $n = 3$  for each group.

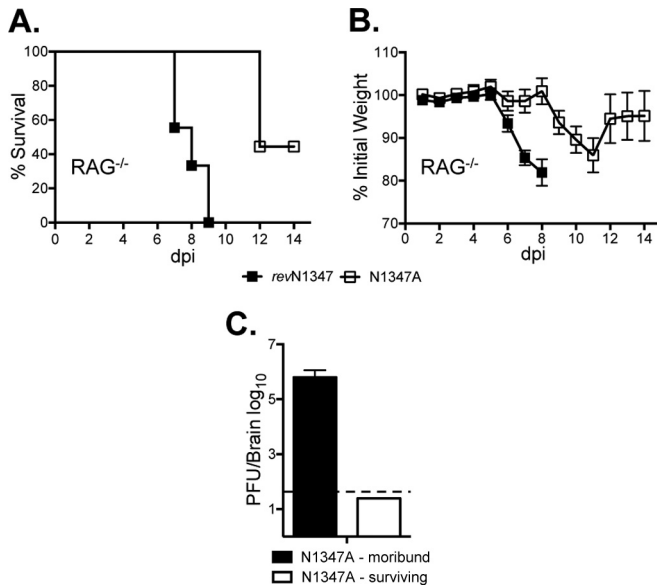


**FIG 8** N1347A is only modestly attenuated in RAG1<sup>-/-</sup> mice. (A and B) Two- to five-month-old RAG1<sup>-/-</sup> male mice were infected intranasally with revN1347 and N1347A and monitored daily for survival and weight loss. Combined results from three independent experiments are shown ( $n = 9$  per group). (C) Brains from RAG1<sup>-/-</sup> mice infected with N1347A that were moribund or recovering were harvested at days 12 and 14, respectively, and viral titers were determined by plaque assay ( $n = 2$  mice per group). The dashed line indicates the limit of detection.

In addition, we observed a small defect of N1347A virus in tissue culture cells, likely in RNA accumulation. This defect was subtle but significant, for in coinfections with WT virus, N1347A was quickly outcompeted. While other reports generally have not concluded that there is a replication defect in cells infected with virus mutated in the macrodomain catalytic site, careful analysis of viral growth kinetics in these reports often shows a subtle delay in viral progeny production after mutant virus infection (17, 18).

In mice, we observed that infection with N1347A virus resulted in significantly reduced viral loads, lower expression levels of pro-inflammatory cytokines, and reduced recruitment of innate immune cells, most notably macrophages, in the brain. However, attenuation was not complete since N1347A caused weight loss in IFNAR<sup>-/-</sup> mice and lethality in RAG1<sup>-/-</sup> mice. This relative lack of sensitivity to the absence of IFN signaling but significant mortality in RAG1<sup>-/-</sup> mice was not expected. Several studies have shown that IFNAR<sup>-/-</sup> mice rapidly succumb to infection with virulent and attenuated strains of MHV (44) (39), suggesting that N1347A is highly attenuated. In contrast, RAG1<sup>-/-</sup> mice infected with the attenuated J2.2-V-1 strain of MHV remain asymptomatic for several weeks before succumbing to the infection (43), while SCID mice can survive for several months if treated with small amounts of anti-spike protein antibody at the time of infection with JHMV (45). Reversion of the N1347A mutation, if it occurred during persistence, could explain disease in infected RAG1<sup>-/-</sup> mice, but we found that this mutation was still present in virus isolated from mice that succumbed to infection at day 12 p.i. (data not shown). Furthermore, virus isolated from RAG1<sup>-/-</sup> mice that succumbed to N1347A infection was still attenuated when inoculated intracranially into wild-type mice, demonstrating that it had not regained virulence (data not shown). Thus,

further work will be required to determine the basis of these apparently anomalous results.

Despite numerous structural and phenotypic studies, the function of the macrodomain during infection remains unclear, as does the reason that coronaviruses have evolved to universally encode this domain. This is partly due to the large diversity of functions ascribed to cellular macrodomains as well as to the lack of reagents to study many of these potential functions (4). The coronavirus macrodomain is an ADP-ribose-1''-phosphatase and also binds to poly(ADP-ribose) (PAR) (12). However, mutation of the catalytic site created as described here and in other reports is highly unlikely to affect the ability of the protein to bind PAR, suggesting that the phenotypes in these reports are due to the loss of enzymatic activity of the macrodomain (15, 16). Why these viruses would evolve to require dephosphorylation of Appr-1''-p or, less likely, an increase in ADR levels is completely unknown. It should be noted that ADR levels can be affected by multiple pathways (46), so ADR produced as a result of the ADR-1''-phosphatase reaction is not likely to change its levels substantially. Another issue is that Appr-1''-p production during coronavirus infection has never been demonstrated, in part because an Appr-1''-p standard is no longer available. This also makes it difficult to determine its role in viral replication. Our results suggest that the mutant virus has a slight defect in RNA accumulation, and one hypothesis is that Appr-1''-p interferes with replication by binding to the RNA polymerase or other enzymes involved in replication. Since the macrodomain is part of nsp3, which is a transmembrane protein embedded as a component of the replicase complex, it makes sense that its function would be required for optimal viral RNA replication. Evaluation of this hypothesis will require additional reagents including Appr-1''-p standards.

Alternatively, the coronavirus macrodomain may be a deMARRYlating enzyme. It was recently found that several other macrodomains have the ability to remove mono-ADP-ribose from proteins (6–8). Poly- and mono-ADP-ribosylation are common posttranslational protein modifications added to proteins by ADP-ribosyltransferases that can alter or change the function of these proteins. These modifications often need to be reversed to allow full functionality of the modified protein (5). In addition, the residues required for deMARRYlation by macrodomains are very similar to those required for phosphatase activity (8). It will be important to determine whether coronavirus macrodomains also contain the ability to deMARRYlate proteins and whether this may be the mechanism by which the macrodomain enhances viral replication or pathogenesis.

## ACKNOWLEDGMENTS

We thank Craig Fett for excellent technical assistance, Wendy Maury, Pat Sinn, and members of their labs for helpful discussions and valuable advice, Keith Jarosinski, Greg Smith, and Dong Yu for sharing of reagents, the University of Iowa Center for Immunology and the Levitt Center for Virology for continued support, and Susan Weiss and Wendy Maury for critical readings of the manuscript.

This study was supported by Public Health Service grants NS36592 (S.P.) and AI-060021 (J.M.P.) and by a grant from the National Multiple Sclerosis Society (RG2864) to S.P. A.R.F. is supported by Institutional NRSA Training Grant T32-AI007260 and an individual NIH NRSA F32-AI113973.

## REFERENCES

1. Perlman S, Netland J. 2009. Coronaviruses post-SARS: update on replication and pathogenesis. *Nat Rev Microbiol* 7:439–450. <http://dx.doi.org/10.1038/nrmicro2147>.
2. Weiss SR, Navas-Martin S. 2005. Coronavirus pathogenesis and the emerging pathogen severe acute respiratory syndrome coronavirus. *Microbiol Mol Biol Rev* 69:635–664. <http://dx.doi.org/10.1128/MMBR.69.4.635-664.2005>.
3. Neuman BW, Joseph JS, Saikatendu KS, Serrano P, Chatterjee A, Johnson MA, Liao L, Klaus JP, Yates JR, III, Wuthrich K, Stevens RC, Buchmeier MJ, Kuhn P. 2008. Proteomics analysis unravels the functional repertoire of coronavirus nonstructural protein 3. *J Virol* 82:5279–5294. <http://dx.doi.org/10.1128/JVI.02631-07>.
4. Han W, Li X, Fu X. 2011. The macro domain protein family: structure, functions, and their potential therapeutic implications. *Mutation Res* 727: 86–103. <http://dx.doi.org/10.1016/j.mrrev.2011.03.001>.
5. Feijs KL, Forst AH, Verheugd P, Luscher B. 2013. Macrodomein-containing proteins: regulating new intracellular functions of mono-(ADP-ribosyl)ation. *Nat Rev Mol Cell Biol* 14:443–451. <http://dx.doi.org/10.1038/nrm3601>.
6. Sharifi R, Morra R, Appel CD, Tallis M, Chioza B, Jankevicius G, Simpson JA, Matic I, Ozkan E, Golia B, Schellenberg MJ, Weston R, Williams JG, Rossi MN, Galehdari H, Krahn J, Wan A, Trembath RC, Crosby AH, Ahel D, Hay R, Ladurner AG, Timinszky G, Williams RS, Ahel I. 2013. Deficiency of terminal ADP-ribose protein glycohydrolase TARG1/C6orf130 in neurodegenerative disease. *EMBO J* 32:1225–1237. <http://dx.doi.org/10.1038/emboj.2013.51>.
7. Rosenthal F, Feijs KL, Frugier E, Bonalli M, Forst AH, Imhof R, Winkler HC, Fischer D, Caffisch A, Hassa PO, Luscher B, Hottiger MO. 2013. Macrodomein-containing proteins are new mono-ADP-ribosylhydrolases. *Nat Struct Mol Biol* 20:502–507. <http://dx.doi.org/10.1038/nsmb.2521>.
8. Jankevicius G, Hassler M, Golia B, Rybin V, Zacharias M, Timinszky G, Ladurner AG. 2013. A family of macrodomain proteins reverses cellular mono-ADP-ribosylation. *Nat Struct Mol Biol* 20:508–514. <http://dx.doi.org/10.1038/nsmb.2523>.
9. Putics A, Filipowicz W, Hall J, Gorbalenya AE, Ziebuhr J. 2005. ADP-ribose-1<sup>st</sup>-monophosphatase: a conserved coronavirus enzyme that is dispensable for viral replication in tissue culture. *J Virol* 79:12721–12731. <http://dx.doi.org/10.1128/JVI.79.20.12721-12731.2005>.
10. Abelson J, Trotta CR, Li H. 1998. tRNA splicing. *J Biol Chem* 273:12685–12688. <http://dx.doi.org/10.1074/jbc.273.21.12685>.
11. Shull NP, Spinelli SL, Phizicky EM. 2005. A highly specific phosphatase that acts on ADP-ribose 1<sup>st</sup>-phosphate, a metabolite of tRNA splicing in *Saccharomyces cerevisiae*. *Nucleic Acids Res* 33:650–660. <http://dx.doi.org/10.1093/nar/gki211>.
12. Egloff MP, Malet H, Putics A, Heinonen M, Dutartre H, Frangeul A, Gruetz A, Campanacci V, Cambillau C, Ziebuhr J, Ahola T, Canard B. 2006. Structural and functional basis for ADP-ribose and poly(ADP-ribose) binding by viral macro domains. *J Virol* 80:8493–8502. <http://dx.doi.org/10.1128/JVI.00713-06>.
13. Saikatendu KS, Joseph JS, Subramanian V, Clayton T, Griffith M, Moy K, Velasquez J, Neuman BW, Buchmeier MJ, Stevens RC, Kuhn P. 2005. Structural basis of severe acute respiratory syndrome coronavirus ADP-ribose-1<sup>st</sup>-phosphate dephosphorylation by a conserved domain of nsP3. *Structure* 13:1665–1675. <http://dx.doi.org/10.1016/j.str.2005.07.022>.
14. Xu Y, Cong L, Chen C, Wei L, Zhao Q, Xu X, Ma Y, Bartlam M, Rao Z. 2009. Crystal structures of two coronavirus ADP-ribose-1<sup>st</sup>-monophosphatases and their complexes with ADP-Ribose: a systematic structural analysis of the viral ADRP domain. *J Virol* 83:1083–1092. <http://dx.doi.org/10.1128/JVI.01862-08>.
15. Neuvonen M, Ahola T. 2009. Differential activities of cellular and viral macro domain proteins in binding of ADP-ribose metabolites. *J Mol Biol* 385:212–225. <http://dx.doi.org/10.1016/j.jmb.2008.10.045>.
16. Park E, Griffin DE. 2009. The nsP3 macro domain is important for Sindbis virus replication in neurons and neurovirulence in mice. *Virology* 388:305–314. <http://dx.doi.org/10.1016/j.virol.2009.03.031>.
17. Kuri T, Eriksson KK, Putics A, Zust R, Snijder EJ, Davidson AD, Siddell SG, Thiel V, Ziebuhr J, Weber F. 2011. The ADP-ribose-1<sup>st</sup>-monophosphatase domains of severe acute respiratory syndrome coronavirus and human coronavirus 229E mediate resistance to antiviral interferon responses. *J Gen Virol* 92:1899–1905. <http://dx.doi.org/10.1099/vir.0.031856-0>.
18. Eriksson KK, Cervantes-Barragan L, Ludewig B, Thiel V. 2008. Mouse hepatitis virus liver pathology is dependent on ADP-ribose-1<sup>st</sup>-phosphatase, a viral function conserved in the alpha-like supergroup. *J Virol* 82:12325–12334. <http://dx.doi.org/10.1128/JVI.02082-08>.
19. Bergmann CC, Lane TE, Stohlman SA. 2006. Coronavirus infection of the central nervous system: host-virus stand-off. *Nat Rev Microbiol* 4:121–132. <http://dx.doi.org/10.1038/nrmicro1343>.
20. Masters PS, Rottier PJ. 2005. Coronavirus reverse genetics by targeted RNA recombination. *Curr Top Microbiol Immunol* 287:133–159. [http://dx.doi.org/10.1007/3-540-26765-4\\_5](http://dx.doi.org/10.1007/3-540-26765-4_5).
21. Almazan F, Dediego ML, Galan C, Escors D, Alvarez E, Ortego J, Sola I, Zuniga S, Alonso S, Moreno JL, Nogales A, Capiscol C, Enjuanes L. 2006. Construction of a severe acute respiratory syndrome coronavirus infectious cDNA clone and a replicon to study coronavirus RNA synthesis. *J Virol* 80:10900–10906. <http://dx.doi.org/10.1128/JVI.00385-06>.
22. Almazan F, Gonzalez JM, Penzes Z, Izeta A, Calvo E, Plana-Duran J, Enjuanes L. 2000. Engineering the largest RNA virus genome as an infectious bacterial artificial chromosome. *Proc Natl Acad Sci U S A* 97:5516–5521. <http://dx.doi.org/10.1073/pnas.97.10.5516>.
23. Almazan F, DeDiego ML, Sola I, Zuniga S, Nieto-Torres JL, Marquez-Jurado S, Andres G, Enjuanes L. 2013. Engineering a replication-competent, propagation-defective Middle East respiratory syndrome coronavirus as a vaccine candidate. *mBio* 4:e00650-13. <http://dx.doi.org/10.1128/mBio.00650-13>.
24. Yount B, Denison MR, Weiss SR, Baric RS. 2002. Systematic assembly of a full-length infectious cDNA of mouse hepatitis virus strain A59. *J Virol* 76:11065–11078. <http://dx.doi.org/10.1128/JVI.76.21.11065-11078.2002>.
25. Almazan F, Sola I, Zuniga S, Marquez-Jurado S, Morales L, Becares M, Enjuanes L. 2014. Coronavirus reverse genetic systems: infectious clones and replicons. *Virus Res* 189:262–270. <http://dx.doi.org/10.1016/j.virusres.2014.05.026>.
26. Tischer BK, von Einem J, Kaufer B, Osterrieder N. 2006. Two-step red-mediated recombination for versatile high-efficiency markerless DNA manipulation in *Escherichia coli*. *Biotechniques* 40:191–197. <http://dx.doi.org/10.2144/000112096>.
27. Zhou H, Perlman S. 2007. Mouse hepatitis virus does not induce Beta interferon synthesis and does not inhibit its induction by double-stranded RNA. *J Virol* 81:568–574. <http://dx.doi.org/10.1128/JVI.01512-06>.
28. Warming S, Costantino N, Court DL, Jenkins NA, Copeland NG. 2005. Simple and highly efficient BAC recombineering using *galK* selection. *Nucleic Acids Res* 33:e36. <http://dx.doi.org/10.1093/nar/gni035>.
29. Zhao J, Zhao J, Perlman S. 2009. De novo recruitment of antigen-experienced and naive T cells contributes to the long-term maintenance of antiviral T cell populations in the persistently infected central nervous system. *J Immunol* 183:5163–5170. <http://dx.doi.org/10.4049/jimmunol.0902164>.
30. Trujillo JA, Fleming EL, Perlman S. 2013. Transgenic CCL2 expression in the central nervous system results in a dysregulated immune response and enhanced lethality after coronavirus infection. *J Virol* 87:2376–2389. <http://dx.doi.org/10.1128/JVI.03089-12>.
31. Ontiveros E, Kim TS, Gallagher TM, Perlman S. 2003. Enhanced virulence mediated by the murine coronavirus, mouse hepatitis virus strain JHM, is associated with a glycine at residue 310 of the spike glycoprotein. *J Virol* 77: 10260–10269. <http://dx.doi.org/10.1128/JVI.77.19.10260-10269.2003>.
32. Casais R, Thiel V, Siddell SG, Cavanagh D, Britton P. 2001. Reverse genetics system for the avian coronavirus infectious bronchitis virus. *J Virol* 75:12359–12369. <http://dx.doi.org/10.1128/JVI.75.24.12359-12369.2001>.
33. Coley SE, Lavi E, Sawicki SG, Fu L, Schelle B, Karl N, Siddell SG, Thiel V. 2005. Recombinant mouse hepatitis virus strain A59 from cloned, full-length cDNA replicates to high titers in vitro and is fully pathogenic in vivo. *J Virol* 79:3097–3106. <http://dx.doi.org/10.1128/JVI.79.5.3097-3106.2005>.
34. Fazakerley JK, Parker S, Bloom F, Buchmeier MJ. 1992. The V5A13.1 envelope glycoprotein deletion mutant of mouse hepatitis virus type-4 is neuroattenuated by its reduced rate of spread in the central nervous system. *Virology* 187:178–188. [http://dx.doi.org/10.1016/0042-6822\(92\)90306-A](http://dx.doi.org/10.1016/0042-6822(92)90306-A).
35. Ontiveros E, Kuo L, Masters PS, Perlman S. 2001. Inactivation of expression of gene 4 of mouse hepatitis virus strain JHM does not affect virulence in the murine CNS. *Virology* 289:230–238. <http://dx.doi.org/10.1006/viro.2001.1167>.
36. Perlman S, Evans G, Afifi A. 1990. Effect of olfactory bulb ablation on

- spread of a neurotropic coronavirus into the mouse brain. *J Exp Med* 172:1127–1132. <http://dx.doi.org/10.1084/jem.172.4.1127>.
37. Templeton S, Kim TH, O'Malley K, Perlman S. 2008. Maturation and localization of macrophages and microglia during infection with a neurotropic murine coronavirus. *Brain Pathol* 18:40–51. <http://dx.doi.org/10.1111/j.1750-3639.2007.00098.x>.
  38. Rempel JD, Murray SJ, Meisner J, Buchmeier MJ. 2004. Differential regulation of innate and adaptive immune responses in viral encephalitis. *Virology* 318:381–392. <http://dx.doi.org/10.1016/j.virol.2003.09.023>.
  39. Ireland DD, Stohlman SA, Hinton DR, Atkinson R, Bergmann CC. 2008. Type I interferons are essential in controlling neurotropic coronavirus infection irrespective of functional CD8 T cells. *J Virol* 82:300–310. <http://dx.doi.org/10.1128/JVI.01794-07>.
  40. Cervantes-Barragan L, Zust R, Weber F, Spiegel M, Lang KS, Akira S, Thiel V, Ludewig B. 2007. Control of coronavirus infection through plasmacytoid dendritic cell-derived type I interferon. *Blood* 109:1131–1137. <http://dx.doi.org/10.1182/blood-2006-05-023770>.
  41. Chen J, Subbarao K. 2007. The immunobiology of SARS. *Annu Rev Immunol* 25:443–472. <http://dx.doi.org/10.1146/annurev.immunol.25.022106.141706>.
  42. Williamson JS, Stohlman SA. 1990. Effective clearance of mouse hepatitis virus from the central nervous system requires both CD4<sup>+</sup> and CD8<sup>+</sup> T cells. *J Virol* 64:4589–4592.
  43. Wu GF, Perlman S. 1999. Macrophage infiltration, but not apoptosis, is correlated with immune-mediated demyelination following murine infection with a neurotropic coronavirus. *J Virol* 73:8771–8780.
  44. Zust R, Cervantes-Barragan L, Kuri T, Blakqori G, Weber F, Ludewig B, Thiel V. 2007. Coronavirus non-structural protein 1 is a major pathogenicity factor: implications for the rational design of coronavirus vaccines. *PLoS Pathog* 3:e109. <http://dx.doi.org/10.1371/journal.ppat.0030109>.
  45. Pewe L, Xue S, Perlman S. 1997. Cytotoxic T cell-resistant variants arise at early times after infection in C57BL/6 but not in SCID mice infected with a neurotropic coronavirus. *J Virol* 71:7640–7647.
  46. Barkauskaite E, Jankevicius G, Ladurner AG, Ahel I, Timinszky G. 2013. The recognition and removal of cellular poly(ADP-ribose) signals. *FEBS J* 280:3491–3507. <http://dx.doi.org/10.1111/febs.12358>.